Modeling and experimental study of trichloroethylene abatement with a negative direct current corona discharge

Modeling and experimental study of trichloroethylene abatement with a negative direct current corona discharge

Arne M. Vandenbroucke,*[,a] Robby Aerts,[b] Wouter Van Gaens,[b] Nathalie De Geyter,[a] Christophe Leys, [a] Rino Morent [a] and Annemie Bogaerts [b]

a. Department of Applied Physics, Research Unit Plasma Technology, Faculty of Engineering and Architecture, Ghent University, Sint-Pietersnieuwstraat 41, 9000 Ghent, Belgium;

b. Department of Chemistry, Research Group PLASMANT, University of Antwerp, Universiteitsplein 1, 2160 Antwerp, Belgium

* Corresponding author

Phone: +32-(0)9-264.38.38

Fax: +32-(0)9-264.41.98

E-mail: ArneM.Vandenbroucke@UGent.be

Abstract

In this work, we study the abatement of dilute trichloroethylene (TCE) in air with a negative direct current corona discharge. A numerical model is used to theoretically investigate the underlying plasma chemistry for the removal of TCE, and a reaction pathway for the abatement of TCE is proposed. The Cl atom, mainly produced by dissociation of COCl, is one of the controlling species in the TCE destruction chemistry and contributes to the production of chlorine containing by-products. The effect of humidity on the removal efficiency is studied and a good agreement is found between experiments and the model for both dry (5% relative humidity (RH)) and humid air (50% RH). An increase of the relative humidity from 5% to 50% has a negative effect on the removal efficiency, decreasing by ±15% in humid air. The main loss reactions for TCE are with $ClO^{\bullet}$, $O^{\bullet}$ and $CHCl_2$. Finally, the by-products and energy cost of TCE abatement are discussed.

Keywords: Non-thermal plasma, Corona discharge, Volatile organic compound, Trichloroethylene, Modeling

1. INTRODUCTION

Non-thermal plasma (NTP) has attracted increased attention in the field of air purification, especially for the abatement of diluted (<1000 ppm) volatile organic compounds (VOCs) from waste gases and indoor air [1-3]. This large group of chemical compounds has an important value for many industrial processes but their inherent emission into the atmosphere puts increased stress on the condition of our environment and causes medical risks for public health. As a consequence of the increased awareness to ensure and improve air quality, the need for remediation technologies that are more sustainable than existing methods has encouraged researchers to explore new innovative methods [4]. In this regard, NTP has been studied over the last 20 years to overcome the issues of conventional methods to treat low VOC concentrated waste gases [5].

In a NTP, highly accelerated electrons gain sufficient energy to trigger multiple chemical processes such as excitation, ionization and dissociation of bulk gas molecules (N_2, O_2, H_2O). This produces a chemical environment containing reactive species such as ions, radicals and metastables that are capable of converting air pollutants to less harmful products. In an ideal process, these pollutants are mineralized to end-products such as CO_2, H_2O, HX and X_2 with X being a halogen (if this element is present in the target compound). However, due to incomplete oxidation, by-products such as other VOCs, NO_x, aerosols and O_3 can also be formed.

During the last two decades, much progress has been made in terms of reactor design and optimization of operating conditions to increase the effectiveness of the removal process [6,7]. Also, combination of NTP with other technologies such as adsorption or catalysis is increasingly investigated in order to improve the performance of plasma alone systems [8-10]. Due to the creation of multiple reactive species in the active plasma zone, there is however still a lack of insight in the underlying mechanisms and reactions that enable the removal of VOCs. A better understanding of the removal process can yield measures to improve the efficiency and can

enable the synthesis of suitable catalysts for plasma-catalytic applications. Therefore, we have experimentally and theoretically investigated the abatement of dilute trichloroethylene (TCE) in air with a negative direct current (DC) glow discharge. TCE is a widespread pollutant in soils, aquifers and air streams due to the fact that it has been extensively used as a solvent and degreasing agent in many industrial processes. Recently, we have experimentally found that the decomposition of TCE has led to the formation of various by-products, including phosgene, dichloroacetylchloride, trichloroacetaldehyde, HCl, Cl_2, CO, CO_2 and O_3 [11].

In this work, we present a kinetic model for the abatement of TCE. The plasma-chemical model and experimental validation allow us to obtain a better understanding of the chemical processes occurring in the discharge. Moreover, it is possible to derive the degradation pathway of TCE, based on the distribution of intermediates and end-products. To our knowledge, only Evans *et al.* have performed such a study to investigate the abatement of TCE from $Ar/O_2/H_2O$ mixtures with dielectric barrier discharges [12]. However, these gas mixtures are not so relevant for industrial applications. Therefore, we focus on the industrially frequently occurring combination of air waste streams polluted with TCE. For practical applications, the humidity of the air also is an important parameter that affects the removal process significantly [3]. Therefore, the water content of the influent is varied and the outcome on the removal process is investigated.

2. DESCRIPTION OF THE MODEL AND CHEMISTRY

The simulations in this work are performed using the numerical model Global_kin developed by Dorai and Kushner [13]. The plasma reactor is considered as a batch reactor with a uniform concentration of species over the entire reactor volume. More details on the model can be found in the papers by Dorai, Kushner and Aerts et al. [13,14].

In this work, the Global_kin model is extended with a reaction analysis module in order to calculate the absolute contributions of all the relevant reactions to the production and loss of all species. These absolute contributions are then used to automatically draw the chemical pathways with Graphviz [15].

The chemistry used in the model contains 114 species and 1155 reactions. This large number of reactions is needed for the description of a complex medium like air. The air chemistry is already described in Van Gaens et al. [16] and the TCE chemistry in Evans et al. [12]. We have taken into account electrons, various types of ions and neutrals, as well as nitrogen and oxygen excited states. Below, we summarize the major destruction reactions that can take place. A complete list of all the reactions that lead to the destruction of TCE in air included in the model can be found in Table S1 (Supplementary material).

In literature, the destruction of TCE with NTP is described by many possible pathways [3]. The first pathway could be the electron attachment of TCE, leading to its decomposition to C_2HCl_2 and a chlorine anion:

$$C_2HCl_3 + e^- \rightarrow C_2HCl_2 + Cl^- \quad k = 1.5 \times 10^{-13} \text{ cm}^3 \text{ molecule}^{-1} \text{ s}^{-1} \text{ (Te =3 eV)} \qquad (1)$$

However, the electron density of the corona discharge used for this application (see below) is quite low in comparison with other low temperature plasmas such as dielectric barrier discharges [17]. Together with the low rate coefficient of reaction 1, the contribution of this reaction should be limited.

Another possible mechanism is direct dissociation by electrons. Unfortunately, the cross sections for this reaction are not known for TCE. We performed however a study of the direct dissociation by electrons on ethylene and concluded that the contribution was less than one percent [18]. Furthermore, it was stated by Magureanu et al. [19] and Urashima et al. [6] that the

direct process would be unlikely, due to the low concentration of TCE in air, and they suggest that TCE oxidation takes place directly by radicals or via oxidation of negative ions.

The dissociation of TCE can also occur by reaction with atomic oxygen leading to numerous end products:

$C_2HCl_3 + O \rightarrow CHOCl + CCl_2$ $\quad k = 5.7 \times 10^{-13}$ cm³ molecule^{-1} s^{-1} (2)

$C_2HCl_3 + O \rightarrow COCl + CHCl_2$ $\quad k = 8.7 \times 10^{-14}$ cm³ molecule^{-1} s^{-1} (3)

$C_2HCl_3 + O \rightarrow C_2Cl_3 + OH$ $\quad k = 6.3 \times 10^{-15}$ cm³ molecule^{-1} s^{-1} (4)

The rate coefficients are in the same order of magnitude as for the electron attachment process. Atomic oxygen has, however, a longer lifetime than the electrons and the reaction with atomic oxygen is therefore more likely to take place.

Especially in humid air, the dissociation of TCE can also be caused by reaction with hydroxyl radicals:

$C_2HCl_3 + OH \rightarrow CHCl_2 + CHOCl$ $\quad k = 3.1 \times 10^{-13}$ cm³ molecule^{-1} s^{-1} (5)

$C_2HCl_3 + OH \rightarrow C_2Cl_3 + H_2O$ $\quad k = 1.9 \times 10^{-12}$ cm³ molecule^{-1} s^{-1} (6)

$C_2HCl_3 + OH \rightarrow C_2HCl_2OH + Cl$ $\quad k = 2.4 \times 10^{-13}$ cm³ molecule^{-1} s^{-1} (7)

$C_2HCl_3 + OH \rightarrow CHCl_2COCl + H$ $\quad k = 2.4 \times 10^{-14}$ cm³ molecule^{-1} s^{-1} (8)

These rate coefficients are also in the same order of magnitude as for the reactions with oxygen atoms, which suggests that the densities of the reactants again have a major influence on the actual rates of the different dissociation reactions. There is also a possibility that TCE is decomposed by radicals originally produced by TCE, e.g. reactions with Cl or ClO radicals:

$C_2HCl_3 + ClO \rightarrow CHCl_2 + COCl_2$ $\quad k = 3.1 \times 10^{-12}$ cm³ molecule^{-1} s^{-1} (9)

$C_2HCl_3 + Cl \rightarrow C_2Cl_3 + HCl$ $\quad k = 7.3 \times 10^{-16}$ cm³ molecule^{-1} s^{-1} (10)

Reaction 9 has a rate coefficient one order of magnitude higher than the previous reactions. However, these reactions can only be a secondary destruction process. Indeed, the densities of Cl and ClO are very low in the beginning but can increase very fast as Cl is a common dissociation product, although the low rate coefficient of reaction 10 will compensate for the higher density.

A final reaction pathway is the dissociation by metastable nitrogen molecules, which are regarded as dominant dissociation species for VOCs [18-21]. As far as we know, no reaction rate coefficients for TCE with metastable nitrogen are published and therefore we have neglected this pathway in our calculations. The metastable nitrogen species $N_2(A^3\sum^+_u)$ have typically a density of one order of magnitude lower than atomic oxygen in humid air [20]. As a result, the reaction rate coefficient of TCE destruction by $N_2(A^3\sum^+_u)$ should be at least one order of magnitude higher ($\sim 10^{-12}$ cm^3 $molecule^{-1}$ s^{-1}) than the values reported for atomic oxygen. This value can be seen as a critical value for the contribution of nitrogen metastable molecules in the destruction of TCE in air.

As the model used in this work is zero-dimensional, the spatial characteristics of the corona discharge can only be approximated by a variation of power deposition as a function of time, i.e., as one power pulse or by a series of power pulses. Therefore, we distinguish three regions in the corona discharge operating in the glow regime with different values of electron density, based on the calculations made by Callebaut et al. [21]. The first one is the tip of the needle which corresponds to the highest electron density and the shortest pulse duration. The second one corresponds to a zone between the tip and the plate of the corona discharge with an average electron density and pulse duration, while the third region corresponds to the plasma zone at the plate with the lowest electron density and the longest pulse duration. By keeping the total energy deposition fixed for every regime, a comparison can be made between them. Figure 1 represents

the calculated electron density for the 3 regimes, called pin, middle and plate, respectively, as a function of the gas residence time used in the model. The "pin regime" has a pulse duration of 0.04 s, whereas the pulse durations of the "middle regime" and the "plate regime" are 0.08 s and 0.26 s, respectively. The electron density is the highest at the tip ($\pm 10^6$ cm^{-3}) and the lowest at the plate ($\pm 10^5$ cm^{-3}), whereas the electron temperature is more or less constant around 2.5 eV. As illustrated in Figure 1, when the gas flows through the reactor, it passes through five power pulses, corresponding to the five pins of the multi-pin-to-plate corona discharge (see below).

We should point out that the main focus of this work is to identify the reaction mechanism in a complex system with humid air and hydrocarbons. Therefore, the description of the plasma itself is narrowed down to five simple power pulses in a zero-dimensional model.

3 DESCRIPTION OF THE EXPERIMENT

The experimental setup used for the validation is shown in Figure 2. A pressurized air bottle (Air Liquide, Alphagaz 1) delivers air to two mass flow controllers (Bronkhorst ®, El-Flow®). Bubbler systems are used to set the TCE concentration and relative humidity (RH) of the gas stream. The initial TCE concentration and humidity are controlled by changing the flow rate of air through the bubbler system. Experiments are carried out with a total flow rate of 2 L/ min which corresponds to a residence time of 1.47 s.

The multi-pin-to-plate plasma source is based on the concept of a negative DC corona discharge operating in the glow mode. The rectangular duct has a cross section of 40 mm × 9 mm and a length of 200 mm. The plasma source consists of five aligned cathode pins which are positioned 28 mm from each other. The distance between the five cathode pins and the single anode plate is 9 mm. The discharge is powered with a 30 kV/20 mA DC power supply and generated at atmospheric pressure and room temperature. A high voltage probe (Fluke 80 K-40, division ratio 1/1.000) measures the voltage applied to the electrode. The discharge current is

determined by recording the voltage signal across a 100 Ω resistor placed in series between the counter electrode and ground. The anode surface is profiled with hollow spherical surface segments having a radius of curvature of 17.5 mm and a depth of 5 mm.

Fourier transform infrared spectroscopy (Bruker, Vertex 70) is used to determine the in- and outlet concentration of TCE and to qualitatively analyze the formation of by-products. The temperature and air humidity are measured before the inlet of the plasma reactor with a combined temperature/humidity sensor (Testo 445).

4. RESULTS AND DISCUSSION

4.1 Effect of the specific energy deposition on the removal efficiency of TCE

Although we simulate three regimes in the corona discharge, the difference was negligible. Therefore, the following results are shown for the middle regime with a TCE inlet concentration of 570 ppm. To validate the model with experiments, we should compare the simulated results with the experimental data at the same specific energy deposition (SED). However, in a corona discharge the plasma volume is much lower compared to the total reactor volume, and this results in an overestimation of the SED and the electron density reported by [21]. To compensate for this observation in our comparison, the actual plasma volume was estimated by assuming a conic volume between pin and plate. The correction factor for the SED, to compensate for this smaller plasma volume is as follows:

$$\text{Correction factor} = \frac{\text{estimated plasma volume}}{\text{total reactor volume}} = 0.1 \tag{11}$$

This means that an SED of 100 J/L in the experiment is compared with 10 J/L in the model.

Figure 3 represents the calculated and measured removal efficiency (RE) as a *function* of the (experimental) SED for both dry and humid air, corresponding to 5% and 50% relative humidity (RH), respectively.

$$RE\ (\%) = \frac{TCE_{inlet} - TCE_{outlet}}{TCE_{inlet}} \times 100\ \% \quad (12)$$

The model and experiment show good agreement for both dry (5% RH) and humid air (50% RH). We observe an increasing trend in the RE upon higher SED, which is related to the higher density of the radicals responsible for destruction of TCE, i.e. ClO, O and OH. Indeed, these radicals are produced by electron impact reactions with the background gas, and the rates of these reactions rise with higher SED, because of the higher electron density. We will explain this in more detail in the next section.

4.2 Effect of the humidity on the removal efficiency of TCE

The effect of humidity is of great interest because water plays an important role in the underlying plasma chemistry. The presence of water affects the removal process since it can quench active plasma species and can limit the electron density due to its electronegative character [3].

Figure 4 shows the effect of the humidity on the removal efficiency, at an SED of 220 J/L, for both the experiment and the model. We can see that the removal efficiency drops by ±15% as the humidity increases from 5% to 75%. To explain this effect we first need to distinguish which reactions mostly contribute to the net loss of TCE, both in dry and humid air. Figure 5 illustrates the relative contributions of various reactions to the loss of TCE, at an SED of 220 J/L, for both dry and humid air (i.e. 5% and 50% RH, respectively). We did not observe a difference between different values of SED, but some small differences were found between dry and humid air, as shown in Figure 5. It is clear that about 65% and 73% of TCE is destroyed by reaction with either ClO or O radicals, in humid and dry air, respectively. Looking closer into the formation of ClO radicals, the following reaction produces 90% of all ClO:

$$Cl + O_3 \rightarrow ClO + O_2 \quad (13)$$

This means that oxygen atoms actually control the loss of TCE, as they affect the formation of ClO radicals, through the formation of ozone. Indeed the most dominant production of ozone is the third body reaction between atomic and molecular oxygen [16].

$$O + O_2 + M \rightarrow O_3 + M \quad (14)$$

For the loss and the production of atomic oxygen we can distinguish the following effects of humidity, which will influence the actual density. First, water quenches the production of metastable nitrogen molecules (reaction 15), which will reduce the chemical quenching of oxygen molecules (reaction 16), resulting in a lower atomic oxygen density:

$$N_2(A^3\textstyle\sum^+_u) + H_2O \rightarrow N_2 + H_2O \quad (15)$$

$$N_2(A^3\textstyle\sum^+_u) + O_2 \rightarrow O + O \quad (16)$$

Second, the electron density drops upon increasing humidity, due to the electronegative character of water, giving rise to an increase of the total attachment rate with a factor of 4. Eventually this lower electron density results in a drop in the formation of oxygen atoms by electron impact dissociation of oxygen molecules. These two effects are found to be responsible for the lower atomic oxygen density in humid air, as can be observed from the inset of Figure 4. The density almost drops a factor of 2 between dry and humid air (i.e., 5% and 50% RH, respectively), which explains the negative effect of the humidity on the removal efficiency, also illustrated in Figure 4, as well as in Figure 3. Furthermore, a higher humidity increases the number of possible destruction reactions between TCE and OH (see reactions 5–8). These reactions are, however, of minor importance than the reaction with O or ClO radicals, as is obvious from Figure 5. So in general, the most important effect of the increasing humidity is the lower production of ClO, resulting in a drop in the removal efficiency.

The influence of humidity on the removal of VOCs with NTP has been well summarized in [3]. It seems that addition of water vapor has a negative influence on the properties of the discharge irrespective of the VOC chemical structure. However, depending on the VOC structure, the outcome of increasing air humidity can be designated as an enhancement, a suppression or a neutral effect. Futamura et al. have also experimentally investigated TCE abatement with a $BaTiO_3$ packed bed [22] and DBD plasma reactor [23] and found that humidity decreases the abatement with about 15 – 20% and 30 – 60%, respectively. They suggest that energetic electrons are quenched by $^3O_2$ to suppress TCE excitation resulting in an decrease of the efficiency. In a recent study by Trushkin et al. [24], the decomposition of toluene was experimentally and numerically studied with a DC atmospheric pressure glow discharge. The authors report that an increase of the humidity leads to an enhancement of the electric field strength and to a higher OH radical density due to electron impact dissociation of H_2O molecules. The increase in OH radical density is responsible for a higher decomposition of toluene and also leads to a catalytic cycle in which OH acts as catalyst which substantially accelerates the recombination of oxygen atoms and suppresses the formation of ozone. In our study, however, the contribution of OH to the TCE abatement is limited to about 5% in total (Figure 5) whereas reactions with ClO and O radicals contribute to 63% of the TCE loss in humid air.

4.3 Destruction pathway of TCE

In the previous sections we only focus on the species and destruction reactions that contribute to the abatement of TCE. However, in environmental applications the by-products which are formed, are of equal importance due to their possible toxicity. Therefore, we have used a reaction path analyzer which automatically generates the reaction path of the plasma chemistry, illustrating the formation of end- and by-products. Figure 6 depicts the loss pathway in the case

of humid air, based on the loss rates integrated over the residence time. Note that the reaction pathway looks the same for dry air, although the relative contributions will vary slightly (cf. Figure 5), but not in such way that it affects the thickness of the lines in Figure 6. The figure only shows species which are produced by destruction of TCE and other intermediate species (Cl, ClO, …), i.e. the species produced by the background gas (OH, O, O_2, …) are not shown, for the sake of clarity.

Starting from TCE the main loss reactions are with ClO and O (reactions 9 and 2, respectively; see above 10), as well as with $CHCl_2$:

$$C_2HCl_3 + CHCl_2 \rightarrow \quad CHCl_3 + C_2HCl_2 \tag{17}$$

which is in accordance with the net loss contributions shown in Figure 5. Note that these reactions are not important at the very start, because they first need some dissociation of TCE to take place by other (non-Cl related) species as mentioned above, but they soon become dominant.

There is also a significant production of C_2HCl_4, as is clear from Figure 6. This species is mainly formed and destroyed by the reaction of TCE with Cl and its reversed decomposition reaction into TCE and Cl.

$$C_2HCl_3 + Cl_2 \leftrightarrow C_2HCl_4 \tag{18}$$

The rate of production is, however, almost equal to the loss rate, resulting in a net production close to zero. For this reason it does almost not contribute to Figure 5.

Looking at the species predominantly formed by these reactions, i.e. $COCl_2$, $CHCl_2$, CHOCl, CCl_2, $CHCl_3$, C_2HCl_2 and C_2HCl_4, (species in rectangles in Figure 6) we can already distinguish two toxic by-products (red rectangles), i.e. $CHCl_3$ (chloroform) and $COCl_2$ (phosgene). Initially,

$CHCl_3$ will be formed indirectly by reaction 9 producing $CHCl_2$, which will react again with TCE to produce $CHCl_3$ in reaction 17. This reaction also produces C_2HCl_2 which is oxidized by molecular oxygen to form CHOCl, as illustrated in Figure 6.

CHOCl is produced for ± 50% directly from TCE (reaction 2), for ± 30% out of C_2HCl_2 (cf. above), and for ± 20% by the reaction of atomic oxygen with $CHCl_2$, as can be deduced from Figure 6. Eventually, most of the CHOCl is converted into COCl by reaction with ClO; see Figure 6.

Reaction 2 also produces CCl_2 directly from TCE , which reacts further on with atomic and molecular chlorine to CCl_3 for almost 85%. The remaining CCl_2 oxidizes with O or OH radicals to COCl. Note that this pathway is drawn in dash in Figure 6, because the absolute rate is lower than the threshold, as the line thickness of the paths in Figure 6 is proportional to their rates. Eventually, COCl decomposes into Cl and the by-product CO (carbon monoxide). On its turn, CO will be further oxidized by OH radicals to another end-product CO_2 (carbon dioxide).

The Cl atoms, mainly produced by dissociation of COCl, are very important for controlling the TCE destruction chemistry, and largely contribute to the production of Cl-containing by-products. Firstly, 24% of the Cl atoms will interact with HOCl, producing two end-products, i.e. Cl_2 and HCl. Secondly, around 72% reacts with O_3 to form ClO radicals (see reaction 13), which can be used in reaction 9 to destroy TCE (cf. Figure 5). The ClO radicals will also react with CHOCl as described above, producing COCl and HOCl.

Finally, the last loss process of the Cl atoms, which contributes for 4%, is the production of CCl_3 upon reaction with CCl_2 as shown in Figure 6. Indeed, as already mentioned, the loss rate of Cl atoms by the production of C_2HCl_4 is equal to the production rate of Cl atoms by the reverse process, leading to a negligible contribution to the loss of Cl atoms.

Looking further at CCl_3, it reacts with O_2 to form CCl_3O_2. This species is converted back into O_2 and CCl_3 as well, but the forward reaction rate is twice as high as the backward reaction rate. The remaining CCl_3O_2 will react with NO and itself to form CCl_3O radicals together with O_2 or NO_2. The CCl_3O radicals will on their turn decompose in the by-product $COCl_2$ (phosgene) and chlorine atoms.

Finally, we also show the production of the by-product $CHCl_2COCl$ (dichloroacetylchloride, DCAC) in Figure 6, but only in dashed lines as the rates are below the rate threshold used to produce the graph. DCAC can be produced by oxidation of TCE with OH or ClO, producing DCAC, and H or Cl atoms, respectively (see reaction 8 for the oxidation with OH).

4.4 By-products of TCE destruction

In this section, we will discuss the end- and by-products formed during TCE abatement and their effect on the environment and human health. In Table 1, a comparison is made for the by-products, as detected in the experiments (with either MS or FT-IR), and calculated with the model for both dry and humid air at an SED of 300 J/L. For the experiments, absolute concentrations could not be obtained with sufficient accuracy, so we only indicate in the table whether these species were detected or not. The calculation results are listed as relative concentrations, with the sum being equal to 100%, to allow an easy comparison between dry and humid air at different removal efficiencies but at the same SED. The experimental diagnostics and the model show a good agreement on a qualitative level, in the sense that the same products are formed in the model and detected in the experiment, except for TCAA (trichloroacetaldehyde), which could not be calculated by the model, simply because of lack of data.

Table 1 shows that for both dry and humid air the model predicts that phosgene ($COCl_2$) and CO account for about 70% of the formed by-products. Phosgene is a highly toxic acid chloride

that can cause suffocation by inhalation [25]. It is widely used as an industrial reagent and building block in the synthesis of pharmaceuticals and other organic compounds. Dichloroacetylchloride (DCAC) can cause skin irritation and is used as a reagent for the production of agricultural chemicals and other products. Chloroform ($CHCl_3$) is a commonly used solvent and reagent in organic synthesis and can cause dizziness, fatigue, and headache [26]. By placing an caustic scrubber downstream of the plasma reactor phosgene and other chlorinated byproducts can be hydrolyzed into non-toxic substances [27].

We can see some small differences between the relative concentrations obtained in dry and humid air. Indeed, the relative concentration of $COCl_2$ slightly drops at increasing humidity as a result of the suppressing effect on ClO, which affects reaction 9 (see also Figure 5 and the explanation in section 3.2). Also, the relative concentrations of HCl and Cl_2 drop due to the suppressing effect on ClO. On the other hand, the relative concentrations of CO and $CHCl_3$ rise. This effect is also related to ClO, as the drop in ClO density gives rise to other TCE destruction reactions, especially by reaction 17. Humid air favors the total production of COCl which is the main source for CO. In dry air most of the COCl is converted into CO by oxidation with O_2 (19%) and ClO (77%); the same is true for humid air, but the oxidation by O_2 becomes more dominant (29%) in relation with ClO (67%). As a result more CHOCl is produced due to oxidation by O_2 which is again a source for CO (as shown in Figure 6).

In contrast to CO, the relative concentration of CO_2 decreases with increasing humidity. The reason for this behavior is the combination of the slow oxidation process from CO to CO_2 and the lower absolute CO concentration compared to dry air.

4.5 Energy yield

The energy yield of the VOC abatement process is an important parameter that is used to compare the performance of different plasma reactors and operating conditions. The energy yield in g/kWh is calculated as follows:

$$\text{Energy yield} = \frac{C_{in} \times \eta \times M \times 0.15}{\varepsilon} \quad (19)$$

where C_{in} is the initial concentration (ppm) of the VOC with molecular weight M (g/mol), η is the maximum removal efficiency and ε the corresponding energy density (J/L), i.e. the energy deposited per unit volume of process gas. Each calculation is based on the fact that one mole of a gas occupies 24.04 L volume at standard ambient temperature and pressure (293 K and 101325 Pa).

Table 2 compares our result with different studies from literature on TCE abatement with NTP. When we evaluate the energy cost, our plasma reactor can decompose almost 10 g/kWh, which is in the same order as the dielectric barrier discharge (DBD) systems used in [28,30].

Our numerical and experimental study of TCE abatement with a negative DC corona discharge has shown that formation of unwanted and toxic by-products is an issue that has to be addressed in order to meet current emission legislations to reduce air pollution. Nevertheless, these results help to unravel the underlying plasma chemistry that leads to the destruction of TCE with NTP and are therefore useful because there is still a lack of knowledge about these mechanisms. Furthermore, if a plasma system is combined with a heterogeneous catalyst it is also crucial to know the by-product distribution in order to maximize the efficiency of the process through an optimal choice of catalyst. We have therefore examined Mn-based catalysts which have proven to be effective in terms of activity and selectivity [32,33].

5. CONCLUSIONS

In general, we can conclude that TCE abatement is possible with this corona discharge, with removal efficiencies in the order of 20-80%, increasing with energy deposition. Moreover, the removal efficiency drops by about 15% when the relative humidity increases from 5% to 50%. This is explained by the rates of the loss processes of TCE. A good agreement is reached between the calculation results and the experimental data. Furthermore, the overall pathway for the destruction of TCE is elucidated, pointing out which are the most important end-products, and how they are formed. The humidity has some effect on the pathways, and on the relative contributions of the end-products, but the absolute concentrations are not so much different. Finally, the energy yield of our process compares reasonably well with literature results from other NTP studies.

ACKNOWLEDGMENTS

R. Morent acknowledges the support of the Research Foundation Flanders (FWO, Belgium) through a post-doctoral research fellowship.

The research leading to these results has received funding from the European Research Council under the European Union's Seventh Framework Programme (FP/2007-2013)/ERC Grant Agreement n. 279022.

We are also very grateful to M. Kushner and group members for providing the Global_kin code and the useful advice. This work was carried out using the Turing HPC infrastructure at the CalcUA core facility of the Universiteit Antwerpen, a division of the Flemish Supercomputer Center VSC, funded by the Hercules Foundation, the Flemish Government (department EWI) and the Universiteit Antwerpen. Finally, we acknowledge the financial support by an IOF-SBO project of the University of Antwerp.

REFERENCES

[1] Kim HH (2004) Plasma Process Polym 1:91-110

[2] Van Durme J, Dewulf J, Leys C, Van Langenhove H (2008) Appl Catal B: Environ 78:324-333

[3] Vandenbroucke AM, Morent R, De Geyter N, Leys C (2011) J Hazard Mater 195:30-54

[4] Parmar GR, Rao NN (2009) Crit Rev Environ Sci Tec 39:41-78

[5] Nunez CM, Ramsey GH, Ponder WH, Abbott JH, Hamel LE, Kariher PH (1993) Air and Waste 43:242–247

[6] Urashima K, Chang JS (2000) IEEE Trans Dielec Electr Insul 7:602-614

[7] Müller S, Zahn RJ (2007) Contrib Plasma Phys 47:520-529

[8] Vandenbroucke AM, Morent R, De Geyter N, Leys C (2011) J Adv Oxid Technol 14:165-173

[9] Vandenbroucke AM, Morent R, De Geyter N, Leys C (2012) J Adv Oxid Technol 15:232-241

[10] Chen HL, Lee HM, Chen SH, Chang MB, Yu SJ, Li SN (2009) Environ Sci Technol 43:2216-2227

[11] Vandenbroucke AM, Dinh Nguyen MT, Giraudon JM, Morent R, De Geyter N, Lamonier JF, Leys C (2011) Plasma Chem Plasma Process 31:707-718

[12] Evans D, Rosocha LA, Anderson GK, Coogan JJ, Kushner MJ (1993) J Appl Phys 74:5378-5386

[13] Dorai R, Kushner MJ (1999) SAE/SP No. 1999-01-3683:81-88

[14] Aerts R, Martens T, Bogaerts A (2012) J Phys Chem C 116:23257-23273

[15] www.graphviz.org

[16] Van Gaens W, Bogaerts A (2013) J Phys D: Appl Phys 46:275201

[17] Fridman A (Ed.) (2008) Plasma chemistry. Cambridge University Press, New York

[18] Aerts R, Tu X, De Bie C, Whitehead JC, Bogaerts A (2012) Plasma Process Polym 9:994-1000

[19] Magureanu M, Mandache NB, Parvulescu VI (2007) Plasma Chem Plasma Process 27:679-690

[20] Kossyi IA, Kostinsky AY, Matveyev AA, Silakov VP (1992) Plasma Sources Sci Technol 1:207-220

[21] Callebaut T, Kochetov I, Akishev Y, Napartovich A, Leys C (2004) Plasma Sources Sci Technol 13:245-250

[22] Futamura S, Zhang AH, Yamamoto T (1997) J Electrostat 42:51-62

[23] Futamura S, Einaga H, Zhang AH (2001) IEEE Trans Ind Appl 37:978-985

[24] Trushkin AN, Grushin ME, Kochetov IV, Trushkin NI, Akishev YS (2013) Plasma Phys Reports 39:167-182

[25] Gift JS, McGaughy R, Singh DV, Sonawane B (2008) Regul Toxic Pharmac 51:98-107

[26] McCulloch A (2003) Chemosphere 50:1291-1308

[27] Hakoda T, Hashimoto S, Fujiyama Y, Mizuno A (2000) J Phys Chem A 104:59-66

[28] Magureanu M, Mandache NB, Parvulescu VI, Subrahmanyam C, Renken A, Kiwi-Minsker L (2007) Appl Catal B Environ 74:270-277

[29] Morent R, Dewulf J, Steenhaut N, Leys C, Van Langenhove H (2006) J Adv Oxid Technol 9:53-58

[30] Oda T, Takahashi T, Kohzuma S (2001) IEEE Trans Ind Appl 37:965-970

[31] Jiang C, Mohamed AH, Stark RH, Yuan JH, Schoenbach KH (200) IEEE Trans on Plasma Sci 33:1416-1425

[32] Nguyen Dinh MT, Giraudon JM, Lamonier JF, Vandenbroucke A, De Geyter N, Leys C, Morent R (2014) Appl Catal B Environ 147:904-911

[33] Vandenbroucke AM, Mora M, Jimenez-Sanchidrian C, Romero-Salguero FJ, De Geyter N, Leys C, Morent R (2014) Appl Catal B Environ 156:94-100

[34] Van Gaens W, Bogaerts A (2014) Plasma Sources Science & Technology 23:035015

[35] Van Gaens W, Bogaerts A (2014) Journal of Physics D-Applied Physics 47:079502

Table Captions

Table 1 Comparison of the end- and by-products detected in the experiments and predicted with the model for dry and humid air at 300 J/L.

Table 2 Comparison of our study with several other literature results for the abatement of TCE obtained with non-thermal plasma.

Table 1

Comparison of the end- and by-products detected in the experiments and predicted with the model for dry and humid air at 300 J/L.

Product	MS	FT-IR	Relative concentration model dry air (%)	Absolute concentration model dry air (ppm)	Relative concentration model humid air (%)	Absolute concentration model humid air (ppm)
DCAC	✓	✓	1	11	1	5
TCAA	✓		Not included	Not included	Not included	Not included
$COCl_2$	✓	✓	30	390	27	211
$CHCl_3$			8	98	13	99
CO		✓	40	517	44	341
CO_2	✓	✓	2	121	1	7
HCl	✓	✓	9	121	7	59
Cl_2	✓		10	128	7	52

Table 2

Comparison of our study with several other literature results for the abatement of TCE obtained with non-thermal plasma.

Plasma type	Carrier gas	Flow rate (L/min)	Concentration range (ppm)	Energy density (J/L)	Energy yield (g/kWh)	Ref.
DBD	Humid air	0.5	150-200	480	8.1	[28]
Positive corona	Dry air	1.5	100	580	2.2	[29]
DBD	Dry air	0.4	1000	1400	13.7	[30]
Pulsed corona	Dry air	-	100	50	30.9	[31]
Negative corona	Humid air	2	500	180	9.7	own study

Figure captions

Figure 1 Calculated electron density for the 3 regimes (pin, middle and plate) as a function of time, when the gas passes through five pulses corresponding to the five pins of the multi-pin-to-plate corona discharge (see text for more explanation).

Figure 2 Experimental set-up.

Figure 3 Calculated and measured TCE removal efficiency as a *function* of the SED for dry and humid air.

Figure 4 Calculated and measured TCE removal efficiency as a function of the relative humidity, for an SED of 220 J/L. The inset shows the calculated O atom density in both dry and humid air (5% and 50% RH, respectively) for the five pulses.

Figure 5 Calculated relative contributions of the reactions leading to the loss of TCE for dry and humid air at an SED of 220 J/L.

Figure 6 Reaction pathway for the loss processes of TCE in humid air. The pathway in dry air looks very similar. The thickness of the arrows is correlated with the rate of this reaction. (rectangles: species predominantly formed from TCE; ovals: intermediate species; yellow rectangles: stable by-products).

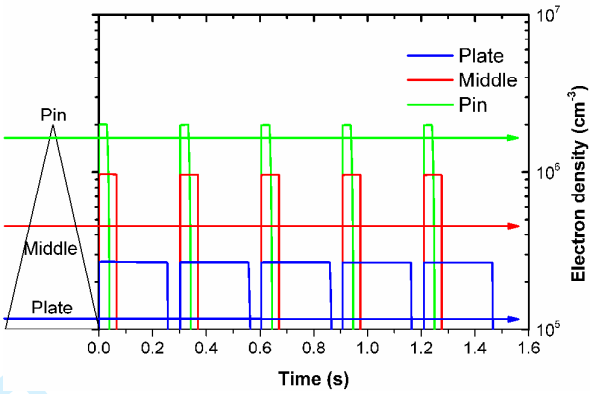

Figure 1

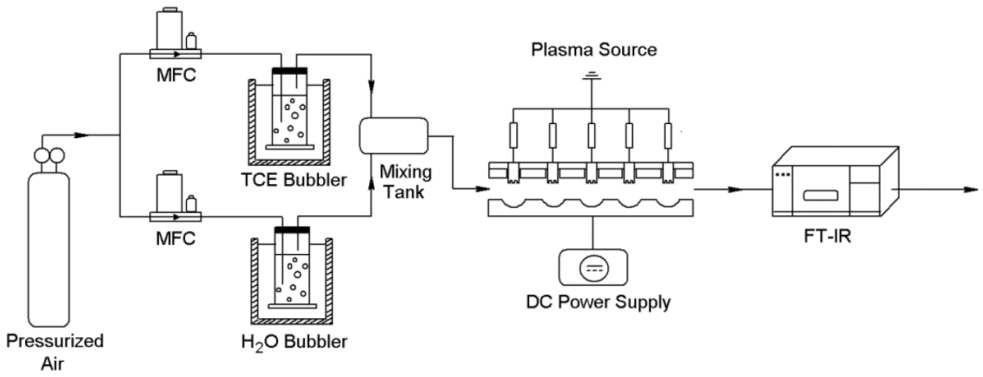

Figure 2

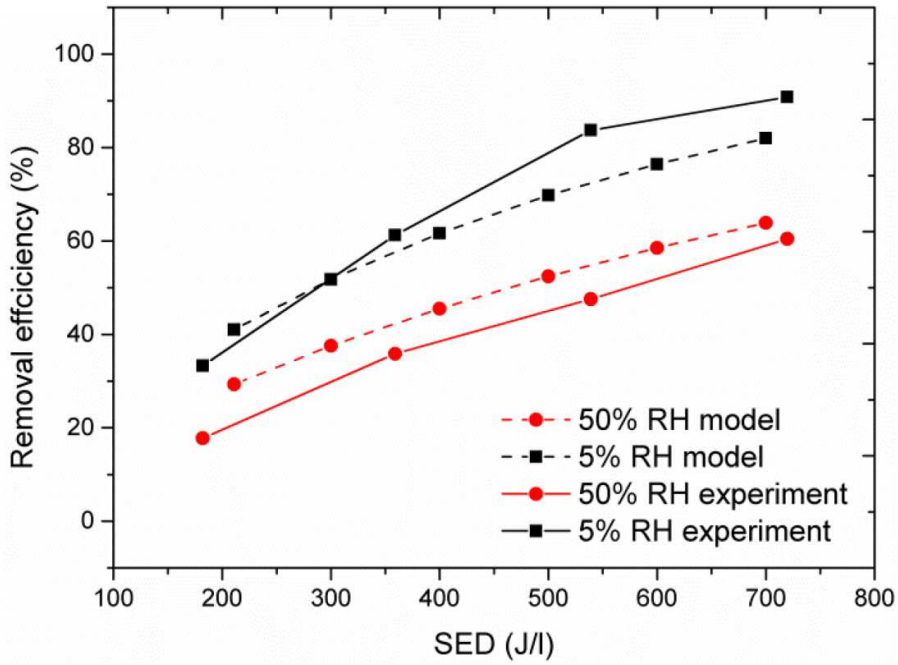

Figure 3

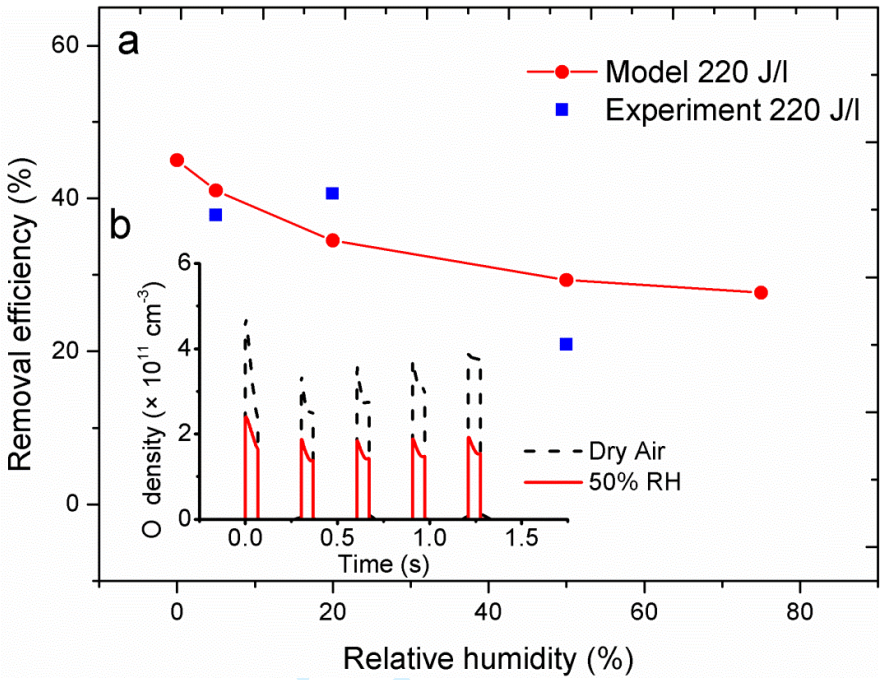

Figure 4

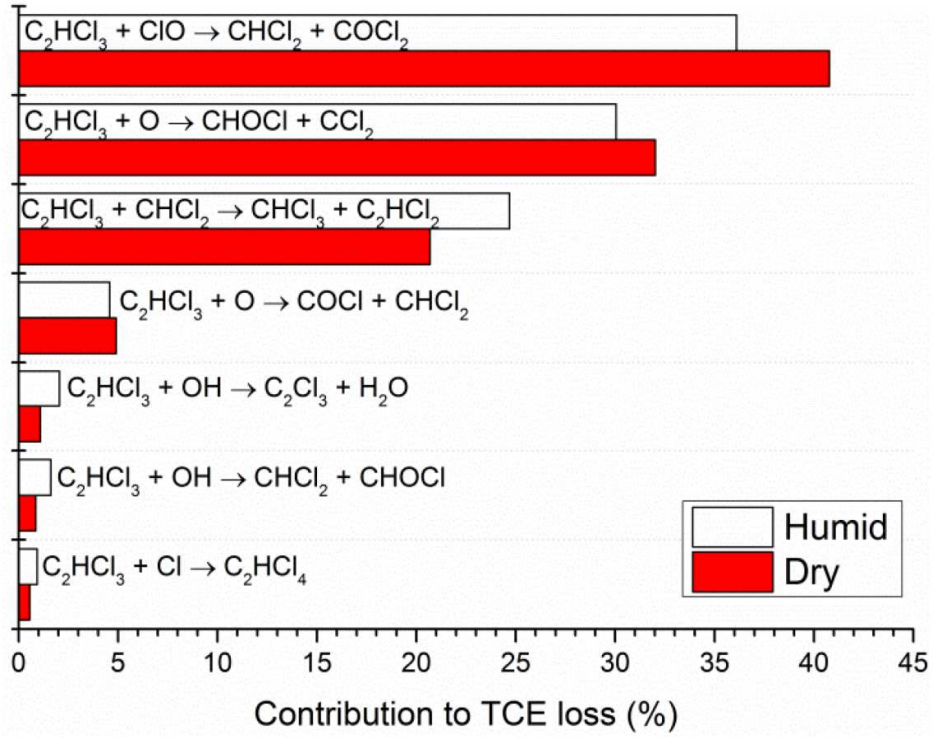

Figure 5

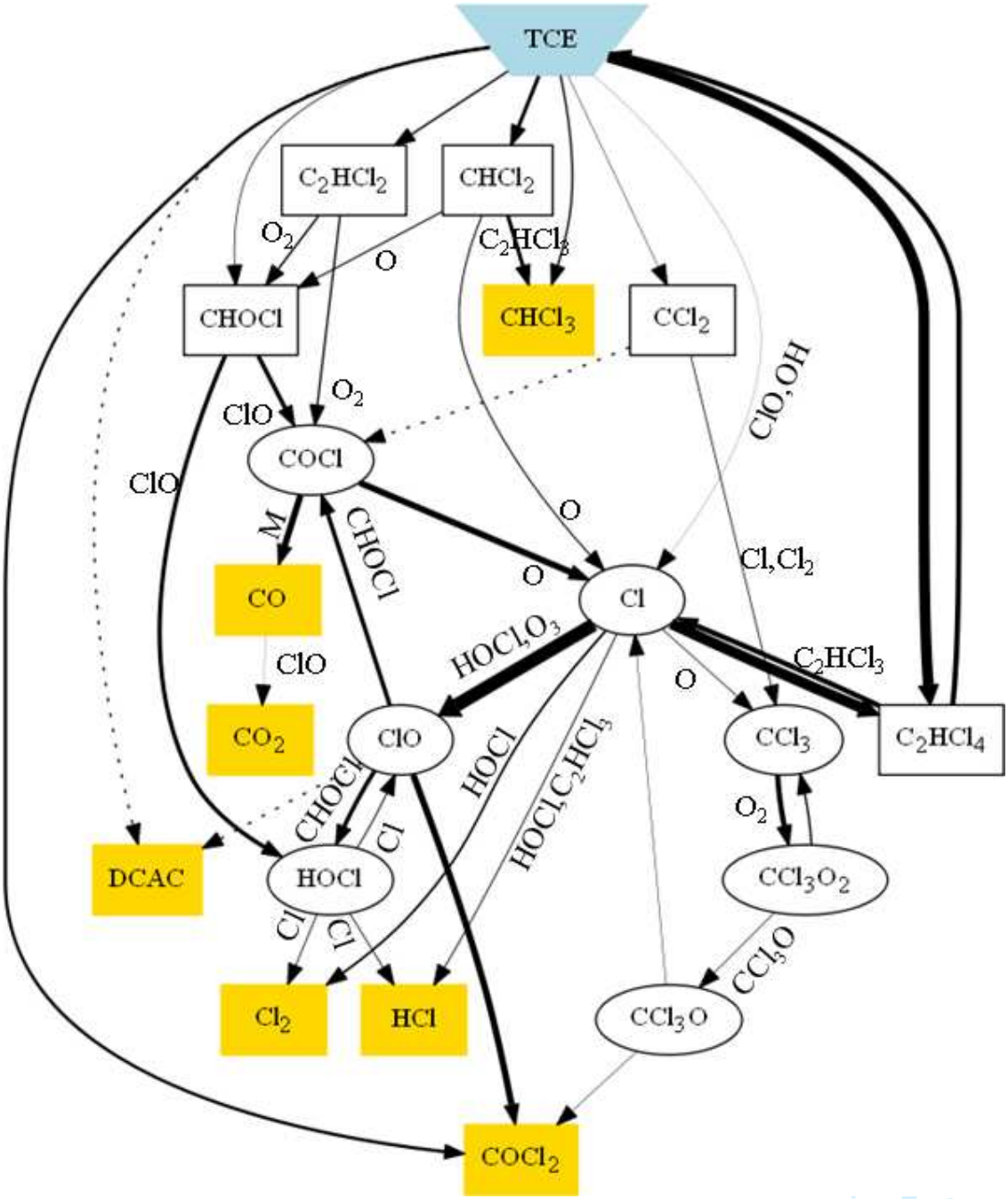
TCE
C2HCl2
CHCl2
O2
O
C2HCl3
CHOCl
CHCl3
CCl2
ClO,OH
ClO
O2
COCl
ClO
M
CHOCl
O
O
Cl
Cl,Cl2
CO
HOCl,O3
C2HCl3
ClO
O
CO2
ClO
CCl3
C2HCl4
HOCl
HOCl,C2HCl3
CHOCl
O2
DCAC
HOCl
Cl
CCl3O2
Cl
Cl
CCl3O
Cl2
HCl
COCl2

Figure 6

Supplementary material

Table S1 Reactions for the TCE destruction included in the model, as well as the corresponding rate coefficients at 300 K and the references where these data were adopted from. Note "a" means that this value is an estimated value and "b" means the rate coefficient is calculated by an online Boltzmann solver in the model, at initialization conditions. The reactions involving the air chemistry can be found in van Gaens et al. [34,35]. The rate coefficients are in units of $cm^3\ s^{-1}$ for the two-body reactions, and in $cm^6\ s^{-1}$ for the three-body reactions.

Modeling and experimental study of trichloroethylene abatement with a negative direct current corona discharge

Plasma Chemistry and Plasma Processing

Arne M. Vandenbroucke,* Robby Aerts, Wouter Van Gaens, Nathalie De Geyter, Christophe Leys, Rino Morent and Annemie Bogaerts

* Corresponding author

Department of Applied Physics, Research Unit Plasma Technology, Faculty of Engineering and Architecture, Ghent University, Sint-Pietersnieuwstraat 41, 9000 Ghent, Belgium

Phone: +32-(0)9-264.38.38

Fax: +32-(0)9-264.41.98

E-mail: ArneM.Vandenbroucke@UGent.be

Supporting information

Table S1: Reactions for the TCE destruction included in the model, as well as the corresponding rate coefficients at 300 K and the references where these data were adopted from. Note "a" means that this value is an estimated value and "b" means the rate coefficient is calculated by an online Boltzmann solver in the model, at initialization conditions. The reactions involving the air chemistry can be found in van Gaens et al. [1,2]. The rate coefficients are in units of $cm^3\ s^{-1}$ for the two-body reactions, and in $cm^6\ s^{-1}$ for the three-body reactions.

#	Reaction	Rate coefficient	Reference
1	$C_2HCl_3 + O_3 > CHOCl + CCl_2 + O_2$	5.00×10^{-20}	[3]
2	$C_2HCl_3 + Cl > C_2HCl_4$	2.05×10^{-12}	[3]
3	$C_2HCl_4 > C_2HCl_3 + Cl$	1.74×10^{1}	[4]
4	$C_2HCl_3 + Cl > C_2Cl_3 + HCl$	7.32×10^{-16}	[3]
5	$C_2HCl_3 + O > CHOCl + CCl_2$	5.73×10^{-13}	[3]
6	$C_2HCl_3 + OH > CHCl_2 + COCl + H$	2.39×10^{-14}	[3]
7	$C_2HCl_3 + CHCl_2 > CHCl_3 + C_2HCl_2$	9.22×10^{-16}	[3]
8	$C_2HCl_3 + ClO > CHCl_2 + COCl + Cl$	5.73×10^{-15}	[3]
9	$C_2HCl_3 + ClO > CHCl_2 + COCl_2$	3.10×10^{-12}	[3]
10	$C_2HCl_3 + ClO > CCl_3 + CHOCl$	2.24×10^{-21}	[3]
11	$C_2HCl_3 + CCl_3 > CCl_4 + C_2HCl_2$	7.44×10^{-19}	[3]
12	$C_2HCl_3 + OH > CHCl_2 + CHOCl$	3.08×10^{-13}	[3]
13	$C_2HCl_3 + OH > C_2Cl_3 + H_2O$	5.73×10^{-14}	[3]
14	$C_2HCl_3 + OH > C_2HCl_2 + OH + Cl$	2.43×10^{-13}	[5]
15	$C_2HCl_3 + O > COCl + CHCl_2$	8.74×10^{-14}	[5]a
16	$C_2HCl_3 + O > C_2Cl_3 + OH$	6.30×10^{-15}	[5]
17	$C_2Cl_3 + Cl_2 > C_2Cl_4 + Cl$	4.49×10^{-13}	[3]
18	$C_2Cl_3 > C_2Cl_2 + Cl$	4.50×10^{-30}	[3]
19	$CCl_4 + O > ClO + CCl_3$	3.25×10^{-16}	[6]
20	$ClO + H_2 > HCl + OH$	4.98×10^{-16}	[6]
21	$ClO + H_2 > HOCl + H$	1.10×10^{-20}	[6]
22	$ClO + O > Cl + O_2$	2.93×10^{-11}	[6]
23	$ClO + ClO > Cl_2 + O_2$	4.90×10^{-15}	[6]
24	$CCl_4 + OH > HOCl + CCl_3$	4.38×10^{-16}	[6]

25	$HOCl + O > OH + ClO$	6.53×10^{-15}	[6]
26	$HOCl + OH > H_2O + ClO$	5.66×10^{-13}	[6]
27	$CCl_3 + H_2 > CHCl_3 + H$	3.18×10^{-22}	[7]
28	$CCl_3 + O > Cl + COCl_2$	4.15×10^{-11}	[8]
29	$CCl_3 + O_2 + M > CCl_3O_2 + M$	1.20×10^{-30}	[8]
30	$CHCl_3 + OH > H_2O + CCl_3$	1.08×10^{-13}	[8]
31	$CHCl_3 + Cl > HCl + CCl_3$	7.85×10^{-14}	[8]
32	$COCl_2 + O > ClO + COCl$	9.96×10^{-15}	[8]
33	$COCl_2 + O(^1D) > ClO + COCl$	1.00×10^{-10}	[8]
34	$ClO + ClO > Cl + ClOO$	3.40×10^{-15}	[8]
35	$O + HCl > OH + Cl$	1.59×10^{-16}	[8]
36	$OH + HCl > H_2O + Cl$	7.53×10^{-13}	[8]
37	$H + HCl > H_2 + Cl$	4.42×10^{-14}	[8]
38	$Cl + H_2O > OH + HCl$	7.84×10^{-24}	[8]
39	$Cl + H_2 > HCl + H$	1.73×10^{-14}	[8]
40	$OH + Cl > O + HCl$	7.10×10^{-16}	[8]
41	$Cl + O_3 > ClO + O_2$	1.20×10^{-11}	[8]
42	$Cl + CCl_3 > CCl_4$	5.00×10^{-11}	[8]
43	$Cl + HOCl > Cl_2 + OH$	1.95×10^{-12}	[8]
44	$Cl + HOCl > HCl + ClO$	1.95×10^{-12}	[8]
45	$Cl + ClO > O + Cl_2$	3.94×10^{-19}	[8]
46	$CCl_3^+ + H^- > CCl_3 + H$	5.00×10^{-8}	[9]
47	$CCl_3^+ + O^- > CCl_3 + O$	5.00×10^{-8}	[9]
48	$CCl_3^+ + O_2^- > CCl_3 + O_2$	5.00×10^{-8}	[9]
49	$CCl_3^+ + Cl^- > CCl_3 + Cl$	5.00×10^{-8}	[9]
50	$CCl_2^+ + H^- > CCl_2 + H$	5.00×10^{-8}	[9]
51	$CCl_2^+ + O^- > CCl_2 + O$	5.00×10^{-8}	[9]
52	$CCl_2^+ + O_2^- > CCl_2 + O_2$	5.00×10^{-8}	[9]
53	$CCl_2^+ + Cl^- > CCl_2 + Cl$	5.00×10^{-8}	[9]
54	$CCl^+ + H^- > CCl + H$	5.00×10^{-8}	[9]
55	$CCl^+ + O^- > CCl + O$	5.00×10^{-8}	[9]
56	$CCl^+ + O_2^- > CCl + O_2$	5.00×10^{-8}	[9]
57	$CCl^+ + Cl^- > CCl + Cl$	5.00×10^{-8}	[9]
58	$Cl_2^+ + H^- > Cl_2 + H$	5.00×10^{-8}	[9]
59	$Cl_2^+ + O^- > Cl_2 + O$	5.00×10^{-8}	[9]
60	$Cl_2^+ + Cl^- > Cl_2 + Cl$	5.00×10^{-8}	[9]
61	$Cl\wedge + H^- > Cl + H$	5.00×10^{-8}	[9]
62	$Cl\wedge + O^- > Cl + O$	5.00×10^{-8}	[9]
63	$Cl\wedge + O_2^- > Cl + O_2$	5.00×10^{-8}	[9]
64	$Cl\wedge + Cl^- > Cl + Cl$	5.00×10^{-8}	[9]
65	$C\wedge + H^- > C + H$	5.00×10^{-8}	[9]
66	$C\wedge + O^- > C + O$	5.00×10^{-8}	[9]
67	$C\wedge + O_2- > C + O_2$	5.00×10^{-8}	[9]
68	$C\wedge + Cl^- > C + Cl$	5.00×10^{-8}	[9]
69	$CCl_2^{+2} + Cl^- > CCl_2^+ + Cl$	5.00×10^{-8}	[9]

70	$O_2^+ + Cl^- > O_2 + Cl$	5.00×10^{-8}	[9]
71	$O^+ + Cl^- > O + Cl$	5.00×10^{-8}	[9]
72	$H + ClOO > OH + ClO$	5.64×10^{-11}	[8]
73	$Cl + ClOO > Cl_2 + O_2$	8.00×10^{-12}	[8]
74	$Cl + ClOO > ClO + ClO$	8.00×10^{-12}	[8]
75	$Cl + CCl_2 > CCl_3$	5.00×10^{-11}	[8]
76	$H_2O^+ + CCl_4 > CCl_3^+ + Cl + H_2O$	1.00×10^{-9}	[8]
77	$O_2^+ + CCl_4 > CCl_3^+ + Cl + O_2$	1.00×10^{-9}	[8]
78	$O_2^+ + CCl_4 > CCl_3^+ + Cl + O$	1.00×10^{-9}	[8]
79	$CCl_3O_2 > CCl_3 + O_2$	1.42×10^{2}	[8]
80	$CCl_3O_2 + CCl_3 > CCl_3O + CCl_3O$	1.00×10^{-12}	[8]
81	$CCl_3O_2 + CCl_3O_2 > CCl_3O + CCl_3O + O_2$	1.57×10^{-12}	[8]
82	$CCl_3O > COCl_2 + Cl$	1.00×10^{5}	[8]
83	$Cl + HO_2 > HCl + O_2$	3.00×10^{-11}	[8]
84	$CCl_4 + O(^1D) > CCl_3 + ClO$	3.54×10^{-10}	[8]
85	$CCl_3 + OH > HCl + COCl_2$	1.00×10^{-11}	[8]
86	$CCl_2 + O > COCl + Cl$	1.00×10^{-11}	[8]
87	$CCl_2 + OH > HCl + COCl$	1.00×10^{-11}	[8]
88	$CCl + O > COCl$	1.00×10^{-12}	[8]
89	$CCl + OH > HCl + CO$	4.00×10^{-11}	[8]
90	$CCl + O > ClO + C$	8.09×10^{-35}	[8]
91	$COCl + Cl > CO + Cl_2$	8.26×10^{-12}	[8]
92	$COCl + O > CO + ClO$	1.00×10^{-11}	[8]
93	$Cl_2 + OH > HOCl + Cl$	8.46×10^{-14}	[8]
94	$CH_2O + O > HCO + OH$	1.75×10^{-13}	[8]
95	$CH_2O + OH > HCO + H_2O$	1.11×10^{-11}	[8]
96	$CH_2O + OH > H + HCOOH$	2.00×10^{-13}	[8]
97	$CH_2O + H > HCO + H_2$	5.75×10^{-14}	[8]
98	$HCOOH + OH > H_2O + CO_2 + H$	4.80×10^{-13}	[8]
99	$C_2Cl_4 + OH > CHCl_2 + COCl + Cl$	1.64×10^{-13}	[3]
100	$C_2Cl_4 + O > COCl_2 + CCl_2$	3.67×10^{-17}	[3]
101	$C_2Cl_4 + ClO > CCl_3COCl + Cl$	3.67×10^{-17}	[3]
102	$C_2Cl_4 + Cl > C_2Cl_5$	9.34×10^{-12}	[3]
103	$C_2HCl_5 + Cl > C_2Cl_5 + HCl$	1.28×10^{-14}	[3]
104	$C_2Cl_5 > C_2Cl_4 + Cl$	$1.28E\times10^{2}$	[3]
105	$C_2HCl_5 + Cl > C_2HCl_4 + Cl_2$	1.21×10^{-23}	[3]
106	$C_2Cl_6 + Cl > Cl_2 + C_2Cl_5$	4.39×10^{-24}	[3]
107	$C_2HCl_2 + Cl > HCl + C_2Cl_2$	1.94×10^{-12}	[3]
108	$C_2HCl_2 + O_2 > CHOCl + COCl$	3.67×10^{-17}	[3]
109	$C_2Cl_3 + Cl > C_2Cl_4$	6.93×10^{-13}	[3]
110	$C_2Cl_3 + Cl > C_2Cl_2 + Cl_2$	1.26×10^{-14}	[3]
111	$C_2Cl_3 + O_2 > COCl_2 + COCl$	3.67×10^{-17}	[3]
112	$C_2Cl_3 + O_2 > C_2Cl_2 + O + ClO$	1.16×10^{-16}	[3]
113	$C_2Cl_2 + O + Cl > CO + CCl_3$	1.66×10^{-11}	[3]

114	$C_2Cl_3 + O > CO + CCl_3$	1.66×10^{-11}	[3]
115	$C_2Cl_3 + ClO > CO + CCl_4$	1.66×10^{-11}	[3]
116	$CHCl_2\,COCl + Cl > CCl_2\,COCl + HCl$	3.67×10^{-15}	[3]
117	$CHCl_2\,COCl + Cl > CHCl_2CO + Cl_2$	2.25×10^{-23}	[3]
118	$CCl_2\,COCl > CO + CCl_3$	2.21×10^{8}	[3]
119	$CHCl_2\,CO > CHCl_2 + CO$	7.08×10^{-21}	[3]
120	$C_2HCl_4 + Cl > CHCl_2 + CCl_3$	4.08×10^{-20}	[3]
121	C2Cl5 + Cl > $CCl_3 + CCl_3$	4.68×10^{-16}	[3]
122	C2Cl5 + Cl > $C_2Cl_4 + Cl_2$	8.86×10^{-10}	[3]
123	C2Cl5 + O_2 > $CCl_3\,COCl + ClO$	2.79×10^{-21}	[3]
124	$CCl_3COCl + Cl > CCl_3\,CO + Cl_2$	2.25×10^{-23}	[3]
125	$CCl_3CO > CCl_3 + CO$	1.64×10^{7}	[3]
126	$C_2Cl_2 + O_2 > COCl + COCl$	3.67×10^{-17}	[3]
127	$C_2Cl_2 + ClO > CO + CCl_3$	1.66×10^{-12}	[3]
128	$C_2Cl_2 + OH > CO + CHCl_2$	1.66×10^{-12}	[3]
129	$CHCl_3 + O > COCl_2 + HCl$	1.98×10^{-16}	[3]
130	$CHCl_3 + O > CCl_3 + OH$	1.20×10^{-15}	[3]
131	$CHCl_3 + Cl > CHCl_2 + Cl_2$	7.25×10^{-26}	[3]
132	$CCl_3 + Cl_2 > CCl_4 + Cl$	1.71×10^{-16}	[3]
133	$CCl_3 + CCl_3 >$ C2Cl6	8.77×10^{-12}	[3]
134	$CCl_3 + CCl_3 > C_2Cl_4 + Cl_2$	1.04×10^{-5}	[3]
135	$CCl_3 + CHCl_2 >$ C2HCl5	1.72×10^{-11}	[3]
136	$CCl_3 + CHCl_2 > C_2Cl_4 + HCl$	6.96×10^{-15}	[3]
137	$CHCl_2 + O_2 > CHOCl + ClO$	5.63×10^{-32}	[3]
138	$CHCl_2 + O > CHOCl + Cl$	1.66×10^{-10}	[3]
139	$CCl_2 + Cl_2 > CCl_3 + Cl$	5.34×10^{-14}	[3]
140	$CHOCl + M > CO + HCl + M$	9.50×10^{-37}	[3]
141	$CHOCl + O > OH + COCl$	5.00×10^{-13}	[8]
142	$CHOCl + O(^1D) > OH + COCl$	1.00×10^{-10}	[8]
143	$CHOCl + OH > H_2O + COCl$	3.23×10^{-13}	[10]
144	$CHOCl + M > HCO + Cl + M$	5.96×10^{-53}	[3]a
145	$CHOCl + H > HCO + HCl$	3.79×10^{-10}	[3]
146	$CHOCl + H > CH_2O + Cl$	2.00×10^{-7}	[3]
147	$CHOCl + Cl > COCl + HCl$	7.93×10^{-13}	[3]
148	$CHOCl + ClO > COCl + HOCl$	1.23×10^{-8}	[3]
149	$CCl_3 + C_2Cl_2 > C_3Cl_5$	7.00×10^{-17}	[3]
150	$C_3Cl_6 + Cl > C_3Cl_6 + Cl_2$	1.26×10^{-25}	[3]
151	$C_3Cl_7 > C_3Cl_6 + Cl$	2.52×10^{-1}	[3]
152	$CCl_3 + C_2Cl_4 > C_3Cl_7$	3.77×10^{-16}	[7]
153	$C_2Cl_3 + C_2Cl_2 > C_4Cl_5$	8.93×10^{-16}	[3]
154	$C_2Cl_2 + C_4Cl_5 > C_6Cl_7$	3.94×10^{-15}	[3]
155	$C_4Cl_6 + Cl > C_4Cl_5 + Cl_2$	1.99×10^{-26}	[3]
156	$C_2Cl_3 + C_2Cl_4 > C_4Cl_7$	3.03×10^{-16}	[3]
157	$C_4Cl_7 > C_4Cl_6 + Cl$	6.91×10^{-01}	[3]
158	$C_4Cl_6 + C_2Cl_3 > C_6Cl_8 + Cl$	1.55×10^{-13}	[3]

159	$C_6Cl_8 > C_6Cl_6 + Cl_2$	7.17×10^{3}	[3]
160	$N + ClO > NO + Cl$	4.98×10^{-14}	[11]
161	$ClO + CO > CO_2 + Cl$	9.51×10^{-22}	[12]
162	$COCl + M > CO + Cl + M$	2.13×10^{-14}	[3]
163	$COCl + H > CO + HCl$	1.66×10^{-10}	[3]
164	$COCl + OH > CO + HOCl$	1.66×10^{-10}	[3]
165	$COCl + O > CO_2 + Cl$	1.66×10^{-10}	[3]
166	$H + Cl_2 > HCl + Cl$	1.87×10^{-11}	[3]
167	$O + Cl_2 > ClO + Cl$	1.88×10^{-13}	[13]
168	$HO_2 + Cl > OH + ClO$	6.00×10^{-12}	[3]
169	$H + HOCl > HCl + OH$	3.08×10^{-12}	[3]
170	$C_2Cl_3 + M > C_2Cl_2 + Cl + M$	2.82×10^{-29}	[3]
171	$C_2Cl_2 + ClO > C2Cl + Cl_2 O$	9.50×10^{-40}	[3]
172	$C_2Cl_2 + OH > C2Cl + HOCl$	8.09×10^{-18}	[3]
173	$C2Cl + O_2 > COCl + CO$	3.67×10^{-14}	[3]
174	$CHCl + Cl_2 > CHCl_2 + Cl$	3.08×10^{-11}	[3]
175	$ClO + OH > HCl + O_2$	1.56×10^{-12}	[8]
176	$COCl + ClO > CO + Cl_2 O$	1.66×10^{-10}	[3]
177	$COCl + ClO > CO_2 + Cl_2$	1.66×10^{-10}	[3]
178	$H_2O_2 + Cl > HO_2 + HCl$	1.15×10^{-13}	[8]
179	$Cl_2O + O > ClO + ClO$	3.02×10^{-12}	[8]
180	$Cl_2O + OH > HOCl + ClO$	6.50×10^{-12}	[8]
181	$CHCl_2\,COCl + O > CCl_2COCl + OH$	5.00×10^{-13}	[8]
182	$CHCl_2\,COCl + O > CHCl + ClO + COCl$	5.00×10^{-13}	[8]
183	$ClO + O_3 > ClOO + O_2$	1.62×10^{-18}	[8]
184	$ClO + O_3 > Cl + O_2 + O_2$	5.25×10^{-15}	[8]
185	$CCl_3 + O_3 > CCl_3O + O_2$	5.00×10^{-13}	[14]
186	$ClOO + CO > CO_2 + ClO$	3.97×10^{-25}	[3]
187	$ClOO + O > ClO + O_2$	2.27×10^{-11}	[3]
188	$COCl_2 + Cl > COCl + Cl_2$	2.17×10^{-24}	[3]
189	$COCl_2 + OH > COCl + HOCl$	8.09×10^{-20}	[3]
190	$COCl_2 + H > COCl + HCl$	5.73×10^{-13}	[3]
191	$C_2Cl_4 + OH > C_2Cl_3 + HOCl$	2.79×10^{-20}	[3]
192	$C_2Cl_4 + OH > CHCl_2 + COCl_2$	5.73×10^{-13}	[3]
193	$C_2Cl_4 + ClO > CCl_3 + COCl_2$	5.73×10^{-13}	[3]
194	$C_2Cl_4 + Cl > C_2Cl_3 + Cl_2$	1.15×10^{-24}	[3]
195	$C_2HCl_3 + e^- > C_2HCl_3^+ + e^- + e^-$	6.33×10^{-14}	[15]b
196	$C_2HCl_3 + e^- > C_2HCl_2 + Cl^-$	1.43×10^{-13}	[16]b
197	$C_2HCl_3^+ + H^- > C_2HCl_3 + H$	5.00×10^{-8}	[9]a
198	$C_2HCl_3^+ + O- > C_2HCl_3 + O$	5.00×10^{-8}	[9]a
199	$C_2HCl_3^+ + O_2 - > C_2HCl_3 + O_2$	5.00×10^{-8}	[9]a
200	$C_2HCl_3^+ + Cl^- > C_2HCl_3 + Cl$	5.00×10^{-8}	[9]a
201	$ClOO + OH > ClO + HO_2$	2.85×10^{-18}	[17]
202	$OH + CO > CO_2 + H$	1.56×10^{-13}	[18]

REFERENCES

[1] Van Gaens W, Bogaerts A (2014) Plasma Sources Sci Technol 23(3):035015

[2] Van Gaens W, Bogaerts A (2014) J Phys D Appl Phys 47(7):079502

[3] Chang WD, Senkan SM (1989) Environ Sci Technol 23(4):442-450

[4] Benson SW, Weissman M (1982) Int J Chem Kin 14(12):1287-1304

[5] Zhu L (2003) PhD Thesis, New Jersey Institute of Technology

[6] Evans D, Rosocha LA, Anderson GK, Coogan JJ, Kushner MJ (1993) J Appl Phys 74(9):5378-5386

[7] NIST Chemical Kinetics Database - Version 6.0, NIST Standard Reference Database 17 (1994).

[8] Gentile AC (1995) PhD Thesis. University of Illinois

[9] Olson RE, Peterson JR, Moseley J (1970) J Chem Phys 53(9):3391

[10] Atkinson R, Baulch DL, Cox RA, Hampson RF, Kerr JA, Rossi MJ, Troe J (1997) 26(6):1329-1499

[11] Freeman CG, Phillips LF (1968) J Phys Chem 72(8):3028

[12] Louis F, Gonzalez CA, Sawerysyn JP (2003) J Phys Chem A 107(46):9931-9936

[13] Chang WD, Karra SB, Senkan SM (1986) Combust Sci Technol 49(3-4):107-121

[14] Clyne MAA, Coxon JA (1968) Proc Royal Soc London Series - Math Phys Sci 303(1473):207

[15] Hudson JE, Vallance C, Bart M, Harland PW (2001) J Phys B - Atom Mol Opt Phys 34(15):3025-3039

[16] Vasil'ev YV, Voinov VG, Barofsky DF, Deinzer ML (2008) Int J Mass Spec 277(1-3):142-150

[17] Xu ZF, Zhu RS, Lin MC (2003) J Phys Chem A 107(7):1040-1049

[18] Baulch DL, Cobos CJ, Cox RA, Esser C, Frank P, Just T, Kerr JA, Pilling MJ, Troe J, Walker RW, Warnatz J (1992) J Phys Chem Ref Data 21(3):411-734